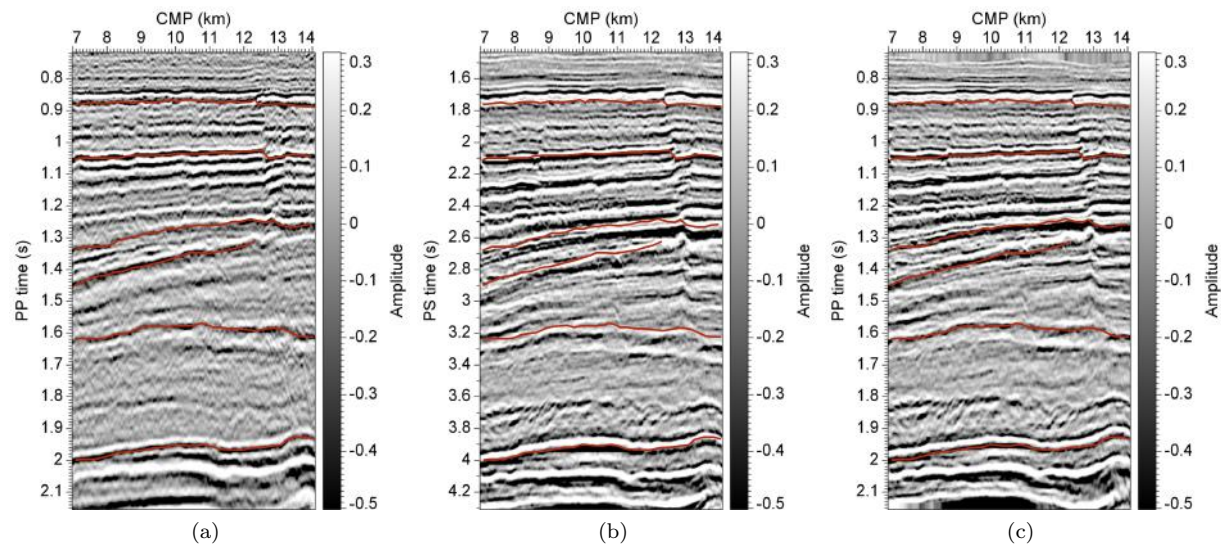


# Automatic registration of PP and PS images using dynamic image warping

Luming Liang & Dave Hale

Center for Wave Phenomena, Colorado School of Mines, Golden, CO 80401, USA



**Figure 1.** Registration of PP and PS images. Apparent misfits between manually picked events (red curves) in the PP image (a), and corresponding events in the PS image (b) are largely reduced after the registration (c) using dynamic image warping. The red curves are placed in the same locations in all three images.

## ABSTRACT

The registration of PP and PS images is a process of correlating corresponding seismic reflections in the two images. We use dynamic image warping to automatically estimate a smooth field of vertical shifts. In warping the PS-image with this shift field, we move reflections in the PS-image to match these in the PP-image. The shift field can also be used to compute the  $V_p/V_s$  ratio. Examples for both synthetic and real data show the effectiveness of this method for seismic image registration.

**Key words:** Seismic image registration; converted-wave;  $V_p/V_s$  ratio; dynamic image warping

## 1 INTRODUCTION

Registering PP and PS images is an important but difficult task in exploration geophysics. Because of differences between propagation and reflection of P waves and S waves, the same geologic layers appear

differently in both positions and waveforms within PP and PS images, as shown in Figure 1a and 1b. The goal of PP and PS image registration is to warp or deform one image to another and thus align them. Useful subsurface information can be extracted from the

estimated warping, e.g., the  $V_p/V_s$  ratio (Fomel et al., 2003; Nickel and Sonneland, 2004; Yuan et al., 2008), which can be used in estimating anisotropic parameters (Grechka et al., 2002) or in building correct migration models (Yan and Sava, 2010).

This registration task is not trivial. First, the registration is based on the assumption that corresponding PP and PS images represent the same subsurface features. However, this assumption is not always valid because P and S waves may respond differently to some reflectors. Second, the process may suffer from cycle skipping, especially when shifts change rapidly. To alleviate these difficulties, manual picking of corresponding features is often used.

We propose an automatic image registration technique that can align PP and PS images. This method is based on a global optimization technique called dynamic image warping (DIW) (Hale, 2012). The output of the dynamic image warping is a vertical-shift field, which can then be used to estimate the  $V_p/V_s$  ratio.

In this paper, both PP and PS images are post-stack time-migrated images.

## 2 THEORY

Registration of a PP image  $f(x, t_{pp})$  and a PS image  $g(x, t_{ps})$  requires a shift field  $u(x, t_{pp})$  such that

$$f(x, t_{pp}) \approx g(x, t_{pp} + u(x, t_{pp})), \quad (1)$$

where  $t_{pp}$  is the PP two-way travel time and  $x$  denotes horizontal CMP distance. Here, we assume the PP and PS images can be aligned with only vertical warping.

From estimates of  $u(x, t_{pp})$ , we can derive the  $V_p/V_s$  ratio. Suppose a reflector located at depth  $z$  appears in the PP image at time  $t_{pp}$  and appears in the PS image at time  $t_{ps}$ . Assuming that  $t_{pp}$  and  $t_{ps}$  are vertical two-way times, we have

$$\begin{aligned} \frac{dt_{pp}}{dz} &= \frac{2}{V_p(z)}, \\ \frac{dt_{ps}}{dz} &= \frac{1}{V_p(z)} + \frac{1}{V_s(z)}, \end{aligned} \quad (2)$$

where  $V_p(z)$  and  $V_s(z)$  are P- and S-wave velocities. Therefore,

$$\frac{dt_{ps}}{dt_{pp}} = \frac{1 + V_p(z(t_{pp}))/V_s(z(t_{pp}))}{2} \quad (3)$$

and

$$\frac{V_p(z(t_{pp}))}{V_s(z(t_{pp}))} = 2 \frac{dt_{ps}}{dt_{pp}} - 1. \quad (4)$$

Let

$$\begin{aligned} V_p(t_{pp}) &\equiv V_p(z(t_{pp})), \\ V_s(t_{pp}) &\equiv V_s(z(t_{pp})), \end{aligned} \quad (5)$$

to obtain  $V_p/V_s$  ratio as a function of  $t_{pp}$  by

$$\frac{V_p(t_{pp})}{V_s(t_{pp})} = 2 \frac{dt_{ps}}{dt_{pp}} - 1. \quad (6)$$

Because S-wave velocities are slower than P-wave velocities, we should compress PS images vertically by a certain factor  $c$  as the first step in registration with corresponding PP images. For the example shown in Figure 1,  $c = 2$ . The relationship between PP time and PS time is

$$t_{ps}(t_{pp}) = c[t_{pp} + u(t_{pp})]. \quad (7)$$

Thus,

$$\frac{dt_{ps}}{dt_{pp}} = c \left( 1 + \frac{du}{dt_{pp}} \right). \quad (8)$$

Combining equation 8 with equation 6, we obtain

$$\frac{V_p(t_{pp})}{V_s(t_{pp})} = (2c - 1) + 2c \frac{du}{dt_{pp}}. \quad (9)$$

Equation 9 relates the partial derivative of the shift field with respect to PP time to the  $V_p/V_s$  ratio. When  $c = 1$ , this result is consistent with those given by Fomel et al. (2003) and Yuan et al. (2008).

Partial derivatives  $\frac{du}{dt_{pp}}$  correspond to time strains (Hale, 2012). The relationship between the  $V_p/V_s$  ratio and the partial derivative  $\frac{du}{dt_{pp}}$  provides a clue about how to set strain limits when using DIW to register PP and PS images. Suppose  $c = 2$ ; if we set the strain limit as 10%, the estimated  $V_p/V_s$  ratio should be within the range of [2.6, 3.4].

## 3 1D SYNTHETIC EXAMPLE

Synthetic 1D PP and PS seismograms are shown in Figure 2a. These seismograms were generated by accumulating Ricker wavelets for some random reflection coefficients.

We denote PP and PS seismograms as  $f(t)$  and  $g(t)$ , respectively, both of which are functions of time:

$$\begin{aligned} f(t) &= \sum_i r_i w(t - t_{pp}(z_i)), \\ g(t) &= \sum_i r_i w(t - t_{ps}(z_i)), \end{aligned} \quad (10)$$

where  $r_i$  is the random reflection coefficient at depth  $z_i$ ,  $t_{pp}(z_i)$  and  $t_{ps}(z_i)$  are the PP and PS reflection times, and  $w(t)$  is the Ricker wavelet. We compute the PP and PS reflection times as follows:

$$\begin{aligned} t_{pp}(z_0) &= 0, \\ t_{ps}(z_0) &= 0, \\ t_{pp}(z_{i+1}) &= t_{pp}(z_i) + 2\delta z/V_p(z_i), \\ t_{ps}(z_{i+1}) &= t_{ps}(z_i) + \delta z/V_p(z_i) + \delta z/V_s(z_i), \end{aligned} \quad (11)$$

where  $\delta z$  is the depth sampling interval,  $V_p(z_i)$  and  $V_s(z_i)$  are specified P- and S-wave velocity functions

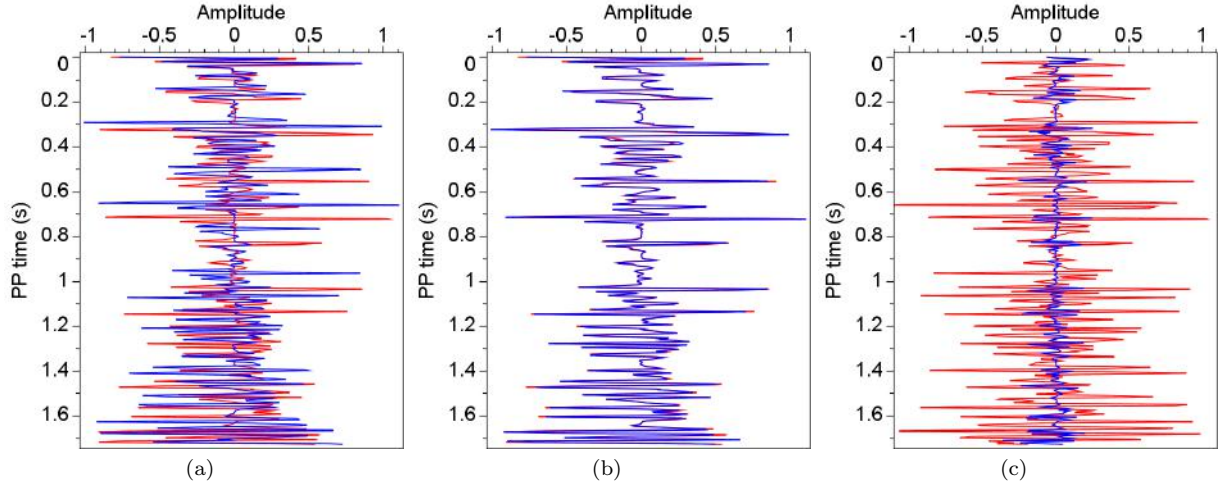


**Figure 2.** Synthetic PP (red) and compressed PS seismogram (blue) before (a) and after (b) warping the PS seismogram with the estimated shift shown in Figure 4. The PS seismogram in (a) is compressed by a factor of  $c = 2$ . Differences (c) between PP and compressed PS seismograms before registration (red) are significantly reduced after registration (blue).

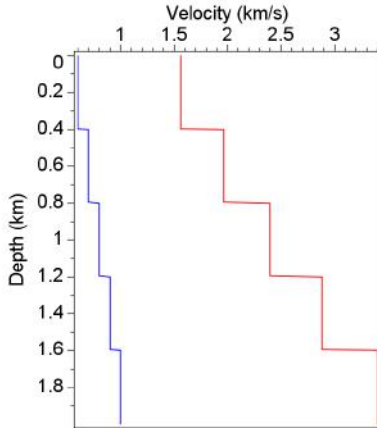


**Figure 3.** Synthetic P-wave (red) and S-wave (blue) velocities.

shown in Figure 3. After we obtain  $f(t)$  and  $g(t)$ , we compress the PS synthetic seismogram by a factor  $c = 2$ , so that both synthetic seismograms have the same number of samples.

Estimating the  $V_p/V_s$  ratio as a function of depth involves three steps:

(1) Estimate shifts  $u(t_{pp})$  that align  $f(t_{pp})$  and  $g(t_{pp})$ , as shown in Figure 4a.

(2) Compute  $V_p/V_s$  ratio as a function of PP time  $\frac{V_p}{V_s}(t_{pp})$  using Equation 9, as shown in Figure 4b. (Note that we have only 1D shifts here.)

(3) Interpolate  $\frac{V_p}{V_s}(t_{pp})$  to get the  $V_p/V_s$  ratio as a function of depth  $\frac{V_p}{V_s}(z)$ , shown as the blue curve in Figure 4c.

In step (1), we use dynamic time warping (Sakoe and Chiba, 1978), the 1D version of dynamic image warping, to estimate the time-variant shifts between two sequences. Dynamic time warping computes a sequence of integer shifts  $u[0 : N - 1]$  between two sequences  $f[i]$  and  $g[i]$  by solving an optimization problem:

$$u[0 : N - 1] = \underset{l[0:N-1]}{\operatorname{argmin}} D(l[0 : N - 1]), \quad (12)$$

where

$$D(l[0 : N - 1]) \equiv \sum_{i=0}^{N-1} (f[i] - g[i + l[i]])^2 \quad (13)$$

subject to

$$\begin{aligned} |u[i] - u[i - 1]| &\leq 1, \\ |u[i]| &\leq L, \end{aligned} \quad (14)$$

where  $N$  is the number of samples in the sequence and  $L$  is a specified maximum shift. The constraint imposed on  $|u[i] - u[i - 1]|$  corresponds to the maximum allowed strain in the estimated shifts. However,  $|u[i] - u[i - 1]| \leq 1$  is a very loose constraint, it implies that 100% strain is permitted. In practice, we modify this constraint to be  $|u[i] - u[i - 1]| + |u[i - 1] - u[i - 2]| + \dots + |u[i - m + 1] - u[i - m]| \leq 1$ , for some integer  $m$ , which approximates a strain limit  $S = 1/m$ .

The integer shifts  $u[0 : N - 1]$  are then smoothed by a Gaussian filter with half-width equal to image sampling intervals divided by the strain limit to obtain the shifts shown in Figure 4a. Derivatives  $\frac{du}{dt_{pp}}$  are computed using a finite-difference approximation.

Figure 2b indicates that, after warping the PS seismogram with the shifts  $u(t_{pp})$  that we find by dynamic time warping, the PP and PS seismograms are well aligned. After alignment, differences between

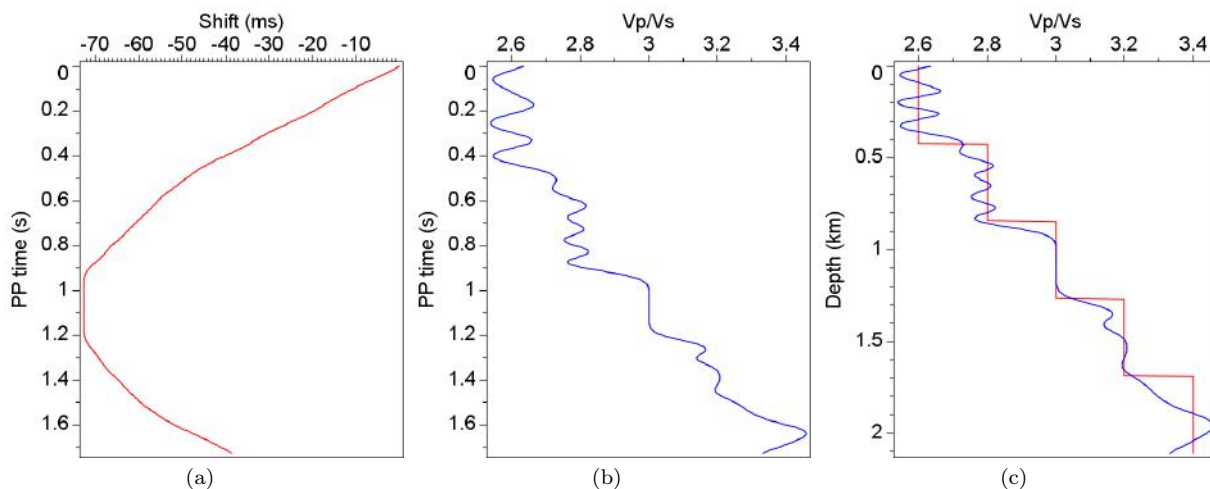


**Figure 4.** Estimated shifts  $u(t_{pp})$  (a) between PP and compressed PS seismograms, corresponding  $V_p/V_s$  ratio (b) as a function of PP time and true (red) and estimated (blue)  $V_p/V_s$  ratios (c) as functions of depth.

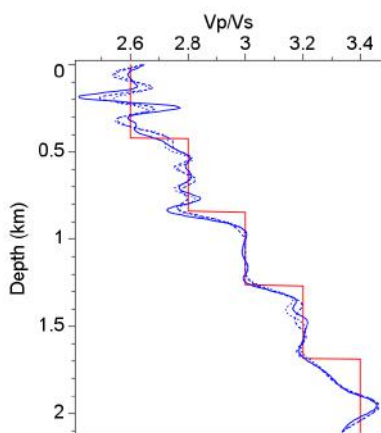


**Figure 5.** True (red) and estimated  $V_p/V_s$  ratios with different strain limits: 25% (dotted blue), 50% (dashed blue) and 100% (solid blue).

PP and PS seismograms are largely reduced, as shown in Figure 2c. Because the PS seismogram is not simply a shifted version of the PP seismogram, we still observe some small differences between the PP and PS seismograms after registration.

In this synthetic example, we chose the compression factor  $c = 2$ . We set the maximum shift  $L = 40$  samples and the strain limit  $S = 25\%$ . In this case, the estimated  $V_p/V_s$  ratio should be in  $[2, 4]$ . The results shown in Figure 2c are consistent with this analysis. Changing the strain limit does not affect the result too much, as shown in Figure 5.

## 4 2D REGISTRATION

Dynamic image warping (DIW) is an extension of 1D dynamic time warping (DTW) to higher dimensions. Because we assume that PP and PS images can be aligned with only vertical warping, we can use the DIW presented by Hale (2012) to estimate the vertical shift field from two images. This method is an improvement over tree-sequential dynamic programming (Mottl et al., 2002; Keyser et al., 2007); more details can be found in Section 4.2 of Hale (2012).

The constraints on the 2D vertical shift field  $u[i, j]$  that we estimate from images are:

$$\begin{aligned}
 & |u[i, j] - u[i, j - 1]| + |u[i, j - 1] - u[i, j - 2]| + \dots \\
 & + |u[i, j - m_1 + 1] - u[i, j - m_1]| \leq 1, \\
 & |u[i, j] - u[i - 1, j]| + |u[i - 1, j] - u[i - 2, j]| + \dots \\
 & + |u[i - m_2 + 1, j] - u[i - m_2, j]| \leq 1, \\
 & |u[i, j]| \leq L,
 \end{aligned} \tag{15}$$

for some integers  $m_1$  and  $m_2$ , which approximates a vertical strain limit  $S_1 = 1/m_1$  and a horizontal strain limit  $S_2 = 1/m_2$ . Here,  $u[i, j]$  is a sampled version of  $u(x, t_{pp})$  in Section 2.  $L$  is again the specified max shift.

To align the PP and PS images shown in Figure 1, we set  $L = 15$  samples,  $S_1$  and  $S_2$  to be 25% and 10%, respectively. The limit of the vertical strain  $S_1 = 25\%$  constrains the  $V_p/V_s$  ratio to be in the range  $[2, 4]$ .

The estimated vertical shift field is shown in Figure 6a. From this shift field we obtained the  $V_p/V_s$  ratio as a function of the PP travel time using equation 9, as shown in Figure 6d. Then, we performed a time-depth conversion similar to the 1D case shown in the previous section to compute the  $V_p/V_s$  ratio as a function of depth.

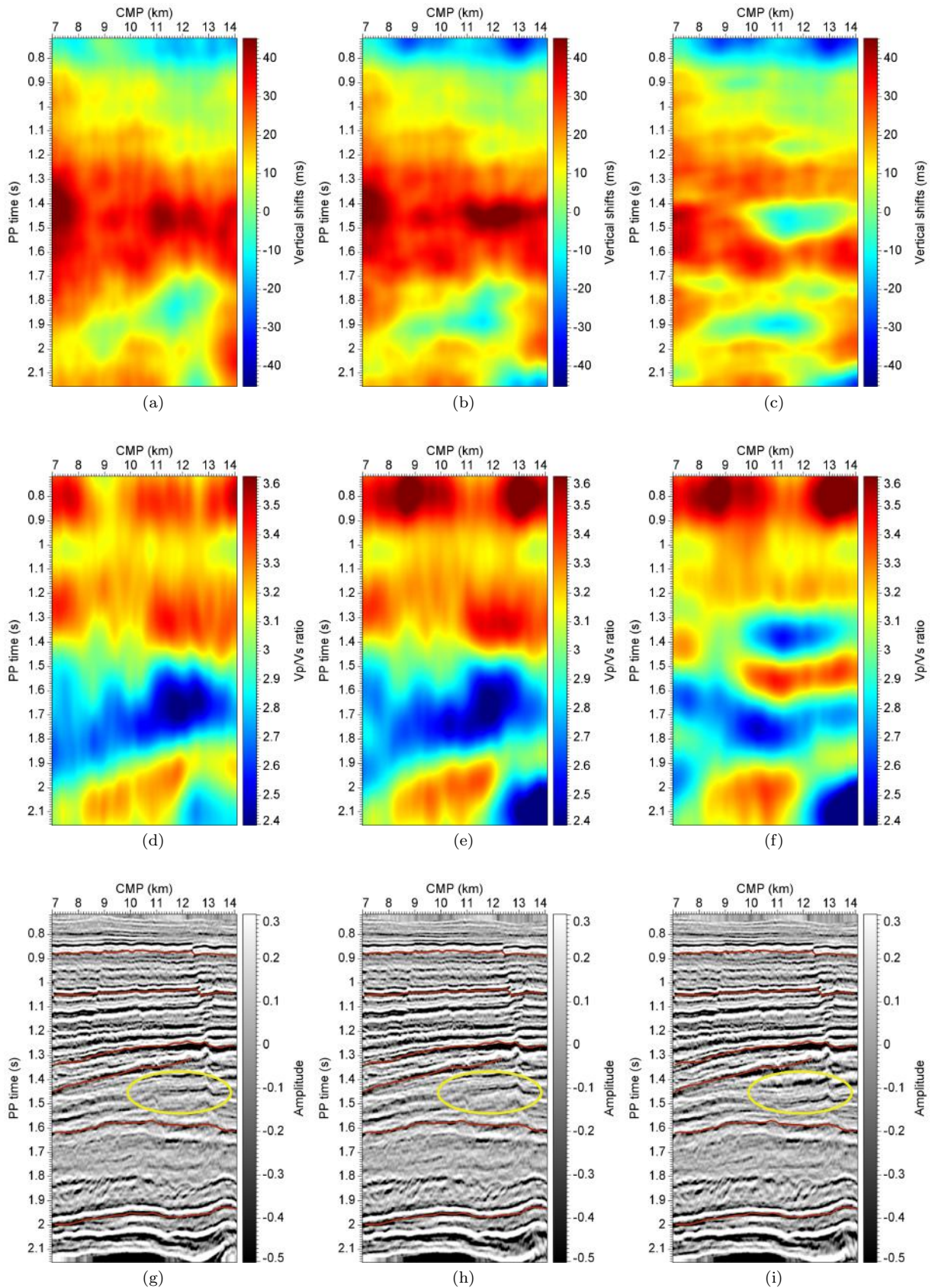


**Figure 6.** Image registration for different time-strain limits. Time shifts computed from PP and PS images shown in Figure 1 with strain limits 25% (a), 50% (b) and 100% (c).  $V_p/V_s$  ratios (d,e,f) computed from those shifts. Warped PS images (g,h,i). All manually picked events (red curves) are placed in the same locations.

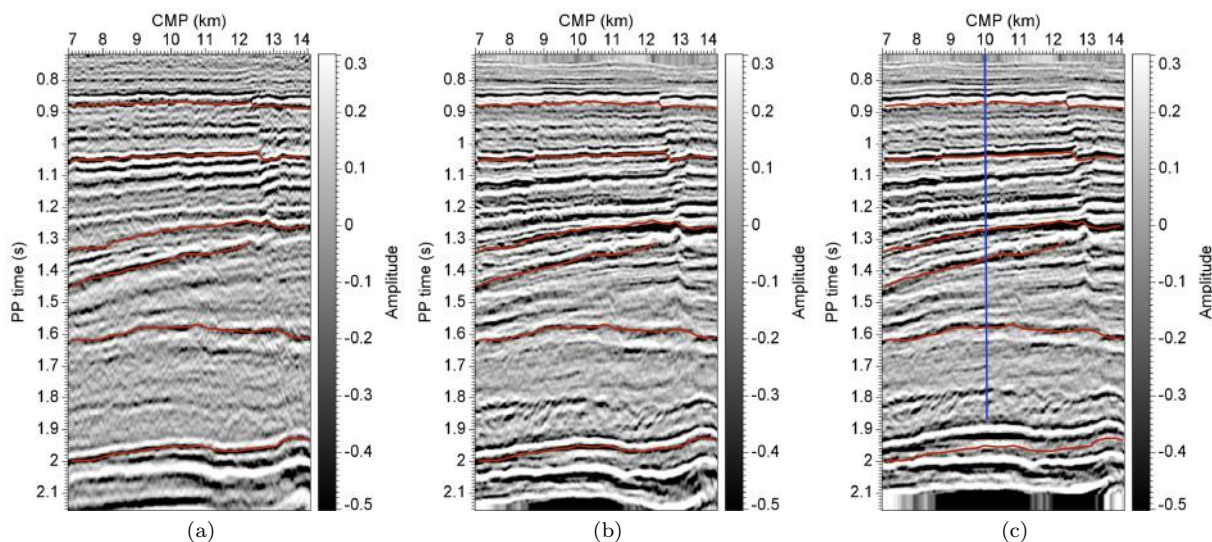


**Figure 7.** The PP image (a), the PS image registered using dynamic image warping (b) and the PS image registered using shifts derived from velocities  $V_p$  and  $V_s$  published by Grechka et al. (2002) at locations along the blue line (c).

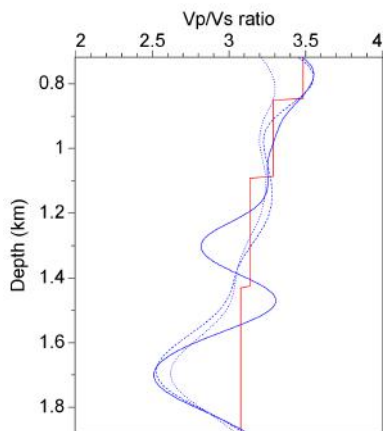


**Figure 8.** A comparison between the  $V_p/V_s$  ratios at CMP = 10 km estimated by our method with strain limits 25% (dotted blue), 50% (dashed blue) and 100% (solid blue) and those cited by Grechka et al. (2002, red).

Registration results with 2 other different vertical strain limits 50% and 100% are also shown in Figure 6. From the warped PS images shown in Figure 6g, h and i, one can see that the registration is generally insensitive to the choice of strain limit. However, some unrealistic deformations appear in Figure 6i (indicated by the yellow oval), suggesting that  $S_1 = 100\%$  is an inadequate constraint.

For comparison, Figure 8 includes a  $V_p/V_s$  function derived from  $V_p$  and  $V_s$  functions provided in Figure 13 of Grechka et al. (2002). Those functions were computed in an inversion using prestack PP, PS and checkshot data. They represented their subsurface model with

piecewise constant parameters, and this representation accounts for the blockiness in the  $V_p/V_s$  curve in Figure 8 that we derived from their results. A visual comparison indicates that the  $V_p/V_s$  ratios computed using a vertical strain limit of 50% in dynamic image warping best match the  $V_p/V_s$  ratios derived from their results.

We can also use the  $V_p/V_s$  ratios from Grechka et al. (2002) with equation 9 to solve for time shifts  $u(t_{pp})$ , which we can then use to warp the PS image to match the PP image. Figure 7c displays the PS image warped in this way alongside the PP image (Figure 7a) and the warped PS image we obtained using DIW (Figure 7b). While our red horizons (located at the same positions in all three of these images) do not correspond exactly to horizons in the blocky model assumed by Grechka et al. (2006), our image registration is comparable to that implied by their model. The only significant differences occur at late times near the bottom of the PS images, where  $V_p$  and  $V_s$  velocities were not specified for their model; there we simply extrapolated  $V_p$  and  $V_s$  velocities to these late times.

## 5 CONCLUSION

Our use of dynamic image warping to register PP and PS images yields vertical shifts that are constrained to not change rapidly in either vertical or horizontal directions. From derivatives of those shifts we may estimate  $V_p/V_s$  ratios.

Our registration method requires that we choose limits for strain, the rates at which shifts may change horizontally and vertically. Although our choices should

depend on image sampling intervals, for stacked seismic images we often observe less variation horizontally, and therefore choose the horizontal strain limit to be lower than the vertical strain limit. In the examples shown in this paper, horizontal and vertical limits of 10% and 50% yielded reasonable registrations.

Our registration for one pair of PP and PS images and  $V_p/V_s$  ratios derived from estimated shifts are consistent with those computed by others, who used a more comprehensive and more time-consuming process to invert for  $V_p$  and  $V_s$ , as well as anisotropy coefficients. Whereas that inversion process began with an interpretation and selection of several key horizons, corresponding to boundaries in a layered subsurface model, our image registration and computation of  $V_p/V_s$  ratios required only the PP and PS images. In this more comprehensive context of seismic inversion, our registration method could be used to facilitate the initial interpretation and correlation of events in PP and PS images.

## ACKNOWLEDGMENTS

We'd like to thank our colleagues for their discussions and feedback on this research. We thank Ilya Tsvankin for providing the images shown in Figure 1. Final thanks to Diane for her help on our writing.

## REFERENCES

- Fomel, S., M. Backus, M. DeAngelo, P. Murray, and B. Hardage, 2003, Multicomponent seismic data registration for subsurface characterization in the shallow gulf of Mexico: Presented at the Offshore Technology Conference.
- Grechka, V., I. Tsvankin, A. Bakulin, C. Signer, and J. O. Hansen, 2002, Anisotropic inversion and imaging of pp and ps reflection data in the north sea: *The Leading Edge*, **21**, 90–97.
- Hale, D., 2012, Dynamic warping of seismic images: CWP Report 723.
- Keysers, D., T. Deselaers, C. Gollan, and H. Ney, 2007, Deformation models for image recognition: *IEEE Transactions on Pattern Recognition and Machine Intelligence*, 1422–1435.
- Mottl, V., A. Kopylov, A. Kostin, A. Yermakov, and J. Kittler, 2002, Elastic transformation of the image pixel grid for similarity based face identification: *Proceedings of the 16th International Conference on Pattern Recognition*, IEEE, 549–552.
- Nickel, M., and L. Sonneland, 2004, Automated ps to pp event registration and estimation of a high-resolution vp-vs ratio volume: Presented at the SEG Expanded Abstracts.
- Sakoe, H., and S. Chiba, 1978, Dynamic programming algorithm optimization for spoken word recognition: *IEEE Transactions on Acoustics, Speech, and Signal Processing*, **26**, 43–49.
- Yan, J., and P. Sava, 2010, Analysis of converted-wave extended images for migration velocity analysis: CWP Report 650.
- Yuan, J. J., G. Nathan, A. Calvert, and R. Bloor, 2008, Automated c-wave registration by simulated annealing: Presented at the SEG Expanded Abstracts.

